Lithium Batteries Hot Paper

DOI: 10.1002/ange.201408124

Excellent Stability of a Lithium-Ion-Conducting Solid Electrolyte upon Reversible Li^+/H^+ Exchange in Aqueous Solutions**

Cheng Ma, Ezhiylmurugan Rangasamy, Chengdu Liang, Jeffrey Sakamoto, Karren L. More, and Miaofang Chi**

Abstract: *Batteries with an aqueous catholyte and a Li metal anode have attracted interest owing to their exceptional energy density and high charge/discharge rate. The long-term operation of such batteries requires that the solid electrolyte separator between the anode and aqueous solutions must be compatible with Li and stable over a wide pH range. Unfortunately, no such compound has yet been reported. In this study, an excellent stability in neutral and strongly basic solutions was observed when using the cubic $Li_7La_3Zr_2O_{12}$ garnet as a Li-stable solid electrolyte. The material underwent a Li^+/H^+ exchange in aqueous solutions. Nevertheless, its structure remained unchanged even under a high exchange rate of 63.6 %. When treated with a 2 M LiOH solution, the Li^+/H^+ exchange was reversed without any structural change. These observations suggest that cubic $Li_7La_3Zr_2O_{12}$ is a promising candidate for the separator in aqueous lithium batteries.*

The imminent exhaustion of fossil-based fuels demands alternative power sources with comparable energy densities.[1–7] Recently, various new battery configurations have been proposed to achieve significantly higher energy densities than the state-of-the-art lithium-ion batteries. Despite the different chemistries, these new batteries frequently have several features in common. Pure Li metal is typically used as the anode to maximize the energy density, as it exhibits the highest possible specific capacity for lithium batteries.[1–4] Additionally, aqueous solutions are often adopted as the "catholyte", because their unique combination of low cost, high reliability, and super-fast Li^+ transport circumvents most of the long-standing issues in the conventional Li-ion batteries.[3–7] Promising batteries showing these characteristics include the aqueous Li–air and Li-redox-flow batteries.[1–4] In particular, the theoretical energy density of the aqueous Li–air battery reaches 2450 $Wh\,kg^{-1}$,[3] which is approximately 10 times of that in the conventional Li-ion battery ($< 300\ Wh\,kg^{-1}$).

To realize long-term operation of aqueous lithium batteries, special attention must be paid to the solid electrolyte separating the Li metal and the aqueous solutions.[1–4] Amongst the many required characteristics, the stability of the solid electrolyte over a wide pH range is particularly desirable, as the amount of H^+ in the aqueous catholyte could vary dramatically during charge/discharge.[1] If the associated pH change deteriorates the performance of the solid electrolyte, the battery can no longer function properly. Beyond this, the ability to adapt to different pH values also provides more options for selecting the aqueous catholytes that can be used with the solid electrolyte.[4] However, few solid electrolytes show satisfactory performance in this regard; many of them (e.g., LiPON and most sulfides) simply decompose in aqueous environments regardless of the pH value.[8,9] Presently, nearly all studies on aqueous Li batteries have utilized a $Li_{1+x+y}Al_xTi_{2-x}P_{3-y}Si_yO_{12}$ (LATP) glass ceramic (Ohara Inc., Japan)[10] as the solid electrolyte,[4,5,7,11–15] which corrodes rapidly unless the pH value is maintained between 7 and 10.[16–20] If immersed in strongly basic solutions, the LATP decomposes and forms a high-resistance phase.[16] This is particularly detrimental for aqueous Li–air batteries, where the pH value could drastically increase upon deep discharge (either by $4Li + O_2 + 4H^+ \rightarrow 4Li^+ + 2H_2O$ or $4Li + O_2 + 2H_2O \rightarrow 4LiOH$).[1] In addition, LATP is chemically unstable against Li, which requires an additional buffer layer to keep it from the anode and thus compromises the overall energy density.[1] These drawbacks necessitate a solid electrolyte that is compatible with Li metal and is stable over a wide pH range.

In this regard, a recently discovered garnet, the cubic $Li_7La_3Zr_2O_{12}$ (LLZO) with the $Ia\bar{3}d$ symmetry,[21–23] appears to show great promise as a solid electrolyte. It not only has a high ionic conductivity of $10^{-4}\ S\,cm^{-1}$, which greatly surpasses that of all the other garnets,[24] but also has excellent stability even in molten Li.[21] Furthermore, unlike many other solid electrolytes, LLZO does not suffer from conductivity degradation upon exposure to humid atmospheres.[21,25] While these unique properties have attracted considerable research interest, the impact of aqueous environments with different pH values on the structure and chemistry of LLZO has not yet been investigated in detail.[26] Based on reported studies, most garnet superionic conductors do not decompose or corrode in

[*] Dr. C. Ma, Dr. E. Rangasamy, Dr. C. Liang, Dr. K. L. More, Dr. M. Chi
Center for Nanophase Materials Sciences
Oak Ridge National Laboratory
1 Bethel Valley Road, Oak Ridge, TN 37831 (USA)
E-mail: mac1@ornl.gov
chim@ornl.gov
Prof. J. Sakamoto
Department of Chemical Engineering and Materials Science
Michigan State University
220 Trowbridge Road, East Lansing, MI 48824 (USA)

[**] The solid electrolyte work was sponsored by the U.S. Department of Energy (DOE), Office of Science, Basic Energy Sciences (BES), Materials Sciences and Engineering Division. The microscopy research was supported by the Center for Nanophase Materials Sciences (CNMS), which is sponsored at Oak Ridge National Laboratory by the Scientific User Facilities Division, BES-DOE. Materials were provided by Michigan State University.

Supporting information for this article is available on the WWW under http://dx.doi.org/10.1002/anie.201408124.

aqueous solutions, but a Li^+/H^+ exchange reaction typically occurs.[27–35] Depending on the pH value, the proton exchange could be intense in certain compounds, leading to the transformation into a different garnet structure and a severe degradation of the ionic conductivity.[27–35] Despite this, the behavior of cubic LLZO in aqueous environments remains an open question. Clearly, the feasibility of utilizing this compound in aqueous lithium batteries cannot be properly evaluated unless its structural and chemical evolutions in aqueous environments are well understood. Specifically, the questions that need to be answered are: 1) Does the cubic LLZO experience a Li^+/H^+ exchange in water like other garnets? 2) Under what range of pH values can LLZO maintain its $Ia\bar{3}d$ structure? 3) Can the changes associated with the Li^+/H^+ exchange be reversed by using aqueous solutions with a higher pH value? 4) How does the Li distribution in the LLZO vary during the proton exchange process?

In this study, using the state-of-the-art scanning transmission electron microscopy (STEM) and electron energy loss spectroscopy (EELS) analysis, we provided answers to all these questions. The Li^+/H^+ exchange reaction with water was observed in hot-pressed (97% relative density), polycrystalline cubic LLZO. In sharp contrast to other garnets, no structural changes occurred even under a high exchange rate of 63.6%. When the LLZO was exposed to a strongly basic solution, the Li^+/H^+ exchange reaction was reversed without any structural change. The excellent stability of the $Ia\bar{3}d$ garnet structure in both neutral and strongly basic environments suggests that cubic LLZO could be a more appropriate solid electrolyte for the aqueous lithium batteries than LATP, which has been the sole extensively used separator to date.

Prior to conducting detailed STEM and EELS analyses, experiments were performed to estimate the time scale of the possible Li^+/H^+ exchange reaction. Powders of cubic LLZO were placed in de-ionized water and stirred at room temperature while the pH value was monitored (Figure S1 in the Supporting Information). The pH value increased almost immediately upon addition of the LLZO powder, and then stabilized in less than one minute. The increase in pH was not accompanied by gas evolution, and X-ray diffraction data (Figure S2) indicated no trace impurity phases that could possibly cause such a dramatic change in pH value. Therefore, the LLZO powder must have taken up a considerable amount of H^+ from the water within a very short time.

Since the pH measurements provided little information regarding the structure and chemistry changes of the material, the EELS analysis was performed (Figure 1). A comparison of the Li-*K* edge before and after exposing the TEM specimen to water revealed a drastic decrease in the Li content; the integrated intensity calculated from the spectra suggested that only 36.4% of the total Li remained in the water-treated specimen. This observation, along with the pH increase in the experiment described above, confirmed that the cubic LLZO experienced a rapid and spontaneous Li^+/H^+ exchange in water. Furthermore, such an exchange was found to be reversible to an extent; after being immersed in a 2 M LiOH solution, the Li content of the protonated LLZO increased, reaching 59.3% of that in the pristine state.

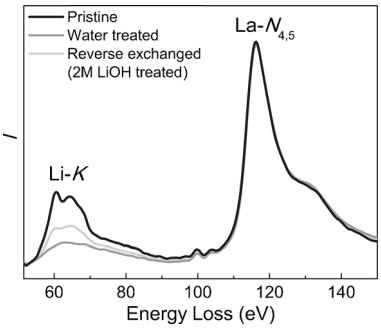

Figure 1. EELS data from pristine, water-treated, and reverse proton exchanged LLZO specimens.

In addition to the edge intensity, the fine structures of Li-*K* edge varied (Figure 1). The Li-*K* edge acquired from the pristine LLZO clearly showed a well-defined doublet, while the water-treated specimen exhibited no such feature. After the reverse exchange in 2 M LiOH solution, this doublet emerged again. As the Li-*K* edge originates from the transition from the 1s to 2p orbitals, its fine structure is very sensitive to the electronic environment of Li.[36] In the $Ia\bar{3}d$ garnet structure, Li ions are distributed among three different sites: the tetrahedral (24*d*), octahedral (48*g*), and the displaced octahedral (96*h*) sites.[22,23,37] As a result, the average electronic environment of Li could be modified under two possible circumstances. It could either be a simple change of the Li distribution among the three differently coordinated sites without any alteration of the $Ia\bar{3}d$ framework, or a structural phase transition that leads to a completely different Li configuration within the lattice. Before reaching a conclusion, the crystal structures and possible grain-boundary phases must be fully interrogated.

Figure 2a shows a typical high-angle annular dark-field (HAADF)-STEM image of the pristine LLZO material along the [001] zone axis. Given that the intensity, *I*, in the HAADF-STEM image is dictated by the atomic number, *Z*, through $I \propto Z^{1.5}$–$Z^{1.8}$,[38] the typical garnet pattern can be straightforwardly identified (see the overlaid atomic model on Figure 2a). After exposure to water, the LLZO showed an increased sensitivity to the electron beam, which prevented the acquisition of

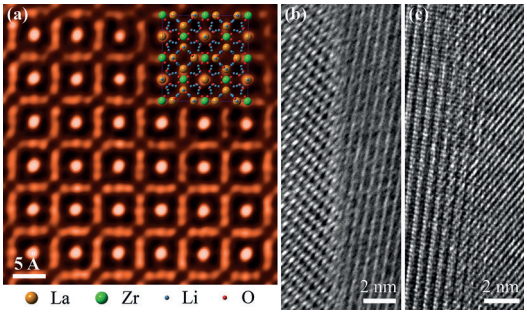

Figure 2. a) HAADF-STEM image of the pristine cubic LLZO along the [001] zone axis (image quality improved with the Butterworth filter). The atomic model is shown as an overlay. b) HRTEM image of a grain boundary in the pristine specimen. c) HRTEM image of a grain boundary after Li^+/H^+ exchange in water.

atomic-resolution HAADF-STEM images. Such beam sensitivity was most likely due to the replacement of the relatively strong Li–O bonds with the weaker O–H···O bonds during Li^+/H^+ exchange in water.[27,28] Under conventional TEM imaging mode, the beam damage can be decreased by spreading the electron beam and lengthening the camera exposure time. Conventional and high-resolution TEM (HRTEM) imaging were thus successfully performed. The low-magnification TEM images indicated no corrosion in either the water- or LiOH-treated LLZO specimens. In addition, the HRTEM study was performed to examine the grain boundaries (Figure 2b,c). Consistent with previous studies,[39] the grain boundaries in the pristine LLZO did not contain any impurities or amorphous phase. After exposure to water and the subsequent 2 M LiOH solution, such a grain-boundary feature remained unchanged; no secondary phase emerged. This observation ruled out the possibility that the Li^+/H^+ exchange was associated with the emergence of any secondary grain-boundary phases.

Several $Ia\bar{3}d$ garnets (isostructural with the cubic LLZO in the present study) transformed to a different crystal structure after the Li^+/H^+ exchange.[27,29] The reported powder X-ray or neutron diffraction patterns of the protonated samples for these garnet compounds were essentially the same, implying that the $Ia\bar{3}d$ garnets experienced the same structural change upon protonation. Nevertheless, two space groups, $I2_13$[27] and $I\bar{4}3d$,[29] had been proposed to describe the structure of the protonated phase. Figure 3 displays the simulated selected area electron diffraction (SAED) patterns for the $Ia\bar{3}d$, $I2_13$, and $I\bar{4}3d$ structures oriented along the [001] zone axis, as well as the SAED patterns collected experimentally from the pristine and protonated LLZO materials. A comparison between the simulated $Ia\bar{3}d$ (Figure 3a) pattern and that of the pristine specimen (Figure 3d) revealed the presence of theoretically prohibited diffraction spots, 00l with $l = 2n$ (indicated by dashed circles) in the latter. Instead of indicating a structure other than $Ia\bar{3}d$, these spots actually resulted from double diffractions, which was evidenced by their absence along another zone axis, [011] (Figure S3).[29] Although the double-diffraction spots should not be used to determine the crystal structure, the three space groups can still be unambiguously distinguished. If the protonated sample belonged to the $I2_13$ or $I\bar{4}3d$ space group, the characteristic diffraction spots (indicated by solid circles in Figure 3b,c) that did not overlap with the double-diffraction spots would emerge. Nevertheless, none of them was present in the SAED pattern of the water-treated specimen (Figure 3e). Clearly, the structural transition associated with the protonation of other garnets,[27,29] no matter which space group it led to, did not take place during the Li^+/H^+ exchange of the cubic LLZO in water. The SAED patterns only indicated a decrease of the lattice parameter from 12.97 to 12.95 Å, implying the protons were present as H^+ rather than the much larger H_3O^+ in the lattice. As for the specimen treated by the 2 M LiOH solution, no additional diffraction spots were observed in the SAED pattern either (not shown here), implying the structure was identical to that of the pristine LLZO specimen. These results suggested the $Ia\bar{3}d$ structure was stable in both neutral and strongly basic solutions.

The structure analysis presented above allowed for a reasonable interpretation of the EELS data in Figure 1. Since the $Ia\bar{3}d$ framework was preserved after immersion in water, the Li-*K* near-edge fine-structure change that signaled a modification of the average electronic environment of Li can only be attributed to the preferential removal of Li from certain sites. Of the three Li sites in the $Ia\bar{3}d$ structure, the displaced octahedral sites (96*h*) are more anisotropic than the other two,[22,23,37] and accommodate 59.6% of the total Li atoms.[23] Since it is commonly agreed that the abundance in the Li-*K* near-edge fine structure reflects an anisotropic electronic environment,[36] the doublet in the Li-*K* edge of the pristine specimen must be primarily caused by the 96*h* site. The prominence of the doublet thus implied the occupancy of such an anisotropic Li site. This is consistent with the exchange rate calculated from the EELS data. After immersion in water, the disappearance of Li-*K* doublet was accompanied by the removal of 63.6% of the total Li from LLZO, and this number happened to be very close to the percentage of Li occupying the 96*h* sites (59.6%).

As such, the interaction between the cubic LLZO and

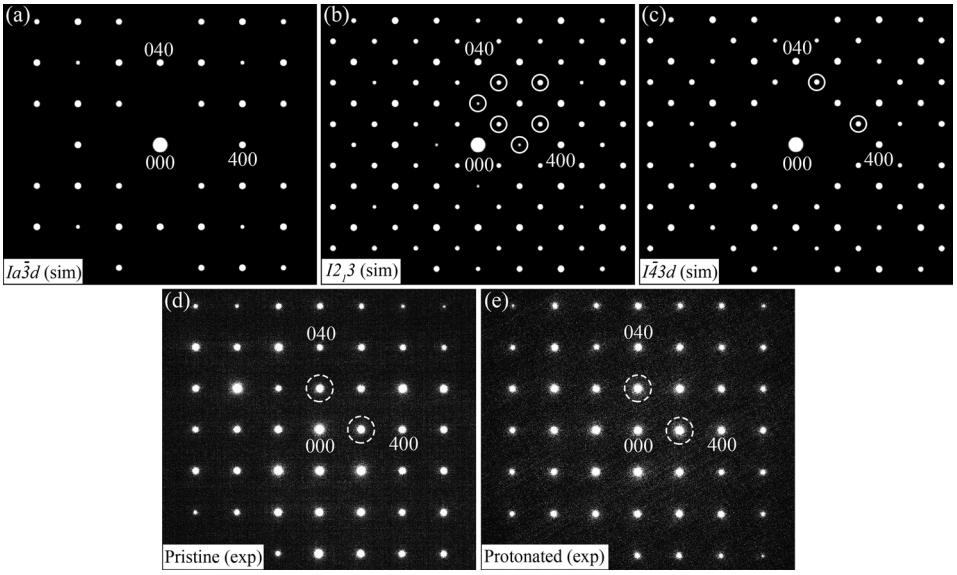

Figure 3. Simulated and experimentally observed SAED patterns along the [001] zone axis. a) Simulated $Ia\bar{3}d$; b) Simulated $I2_13$; c) Simulated $I\bar{4}3d$; d) Experimentally observed pristine specimen; e) Experimentally observed protonated specimen. The characteristic spots for the $I2_13$ and $I\bar{4}3d$ structures are highlighted with solid circles. The double-diffraction spots observed in the experiments are highlighted with dashed circles.

water may be described below. The LLZO experienced a rapid and spontaneous Li^+/H^+ exchange reaction upon exposure to water. The $Ia\bar{3}d$ structure persisted during this process. The proton exchange preferentially occurred at the most anisotropic Li site, 96*h*, leading to the disappearance of the doublet in Li-*K* near-edge fine structure. After the depletion of Li from this site, the exchange barely proceeded further, leaving both 48*g* and 24*d* sites largely unaffected. During this stage, the 48*g* site might be dominant in the exchange, as the 24*d* site was reported to be the least mobile one in the cubic garnets.[30,31] In this way, the final product of the water treatment was most likely a protonated $Ia\bar{3}d$ garnet with its 24*d* sites occupied by Li, 48 *g* sites occupied by Li and a small amount of H, and 96 *h* sites solely occupied by H, as illustrated schematically in Figure 4. This mechanism differs

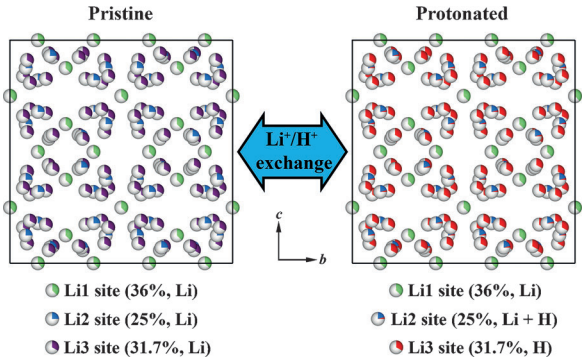

Figure 4. Schematic illustration for the Li^+/H^+ exchange process of cubic LLZO in water. Li1, Li2, and Li3 represent the 24*d*, 48*g*, and 96*h* sites, respectively. The percentage numbers in the parentheses indicate the site occupancy reported in Ref. [23], which is also reflected in the portion of the site symbols that are colored.

significantly from that of other garnets, such as $Li_5La_3Ta_2O_{12}$ and $Li_5La_3Nb_2O_{12}$ (although the exchange rate was comparable),[31] where all three Li sites participated in the protonation.[27,30] Since the 24*d* site was believed to be a "framework site",[30] its minimum involvement in the Li^+/H^+ exchange must have played a critical role in the stability of LLZO. Beyond this, if focusing on the product instead of the detailed reaction process, the only difference between the Li^+/H^+ exchange reactions of the cubic LLZO and that of the other isostructural garnets lies in the fact that LLZO preserved its $Ia\bar{3}d$ structure during protonation. Therefore, it appears reasonable to believe that such a difference in structural stability is primarily responsible for the variation in macroscopic conductivity after the Li^+/H^+ exchange: it must be the persistence of the $Ia\bar{3}d$ structure that assured the cubic LLZO remained free from the severe protonation-induced conductivity degradation[25] that occurred in all the other $Ia\bar{3}d$ garnets.[27–35]

In summary, we have elucidated the microscopic process of the interactions between cubic LLZO and aqueous solutions. The material underwent a reversible Li^+/H^+ exchange reaction in water. In sharp contrast to other garnets, the proton exchange process was not accompanied by any structural transition even under a high exchange rate of 63.6%. When immersed in a 2 M LiOH solution, the Li^+ reentered the lattice by reverse Li^+/H^+ exchange, without causing any structural change. Such an excellent structural stability is believed to be the key to the absence of severe conductivity degradation upon Li^+/H^+ exchange. These results indicated that cubic LLZO could serve as a better solid electrolyte in aqueous Li batteries than LATP, which has been the only material of choice so far.

Received: August 11, 2014
Published online: October 21, 2014

Keywords: catholyte · electron microscopy · lithium batteries · proton exchange · solid electrolytes

[1] M. Balaish, A. Kraytsberg, Y. Ein-Eli, *Phys. Chem. Chem. Phys.* **2014**, *16*, 2801–2822.
[2] P. G. Bruce, L. J. Hardwick, K. M. Abraham, *MRS Bull.* **2011**, *36*, 506–512.
[3] T. Zhang, N. Imanishi, Y. Takeda, O. Yamamoto, *Chem. Lett.* **2011**, *40*, 668–673.
[4] Y. Wang, P. He, H. Zhou, *Adv. Energy Mater.* **2012**, *2*, 770–779.
[5] X. Wang, Y. Hou, Y. Zhu, Y. Wu, R. Holze, *Sci. Rep.* **2013**, *3*, 1401.
[6] J.-Y. Luo, W.-J. Cui, P. He, Y.-Y. Xia, *Nat. Chem.* **2010**, *2*, 760–765.
[7] Y. Zhao, Y. Ding, J. Song, L. Peng, J. B. Goodenough, G. Yu, *Energy Environ. Sci.* **2014**, *7*, 1990–1995.
[8] S. Adams, R. P. Rao, *J. Mater. Chem.* **2012**, *22*, 1426–1434.
[9] C. S. Nimisha, G. M. Rao, N. Munichandraiah, G. Natarajan, D. C. Cameron, *Solid State Ionics* **2011**, *185*, 47–51.
[10] J. Fu, *J. Mater. Sci.* **1998**, *33*, 1549–1553.
[11] Y. H. Lu, J. B. Goodenough, *J. Mater. Chem.* **2011**, *21*, 10113–10117.
[12] Y. H. Lu, J. B. Goodenough, Y. Kim, *J. Am. Chem. Soc.* **2011**, *133*, 5756–5759.
[13] Y. R. Wang, Y. G. Wang, H. S. Zhou, *ChemSusChem* **2011**, *4*, 1087–1090.
[14] Y. Zhao, L. N. Wang, H. R. Byon, *Nat. Commun.* **2013**, *4*, 1896.
[15] N. M. Asl, S. S. Cheah, J. Salim, Y. Kim, *RSC Adv.* **2012**, *2*, 6094–6100.
[16] S. Hasegawa, N. Imanishi, T. Zhang, J. Xie, A. Hirano, Y. Takeda, O. Yamamoto, *J. Power Sources* **2009**, *189*, 371–377.
[17] N. Imanishi, Y. Takeda, O. Yamamoto, *Electrochemistry* **2012**, *80*, 706–715.
[18] Y. Shimonishi, T. Zhang, N. Imanishi, D. Im, D. J. Lee, A. Hirano, Y. Takeda, O. Yamamoto, N. Sammes, *J. Power Sources* **2011**, *196*, 5128–5132.
[19] Y. Shimonishi, T. Zhang, P. Johnson, N. Imanishi, A. Hirano, Y. Takeda, O. Yamamoto, N. Sammes, *J. Power Sources* **2010**, *195*, 6187–6191.
[20] S. D. Jackman, R. A. Cutler, *J. Power Sources* **2013**, *230*, 251–260.
[21] R. Murugan, V. Thangadurai, W. Weppner, *Angew. Chem. Int. Ed.* **2007**, *46*, 7778–7781; *Angew. Chem.* **2007**, *119*, 7925–7928.
[22] J. T. Han, J. L. Zhu, Y. T. Li, X. H. Yu, S. M. Wang, G. Wu, H. Xie, S. C. Vogel, F. Izumi, K. Momma, Y. Kawamura, Y. Huang, J. B. Goodenough, Y. S. Zhao, *Chem. Commun.* **2012**, *48*, 9840–9842.
[23] Y. T. Li, J. T. Han, C. A. Wang, S. C. Vogel, H. Xie, M. W. Xu, J. B. Goodenough, *J. Power Sources* **2012**, *209*, 278–281.
[24] E. J. Cussen, *J. Mater. Chem.* **2010**, *20*, 5167–5173.

[25] M. A. Howard, O. Clemens, E. Kendrick, K. S. Knight, D. C. Apperley, P. A. Anderson, P. R. Slater, *Dalton Trans.* **2012**, *41*, 12048 – 12053.
[26] Y. Shimonishi, A. Toda, T. Zhang, A. Hirano, N. Imanishi, O. Yamamoto, Y. Takeda, *Solid State Ionics* **2011**, *183*, 48 – 53.
[27] C. Galven, J. Dittmer, E. Suard, F. Le Berre, M. P. Crosnier-Lopez, *Chem. Mater.* **2012**, *24*, 3335 – 3345.
[28] C. Galven, J.-L. Fourquet, M.-P. Crosnier-Lopez, F. Le Berre, *Chem. Mater.* **2011**, *23*, 1892 – 1900.
[29] C. Galven, E. Suard, D. Mounier, M. P. Crosnier-Lopez, F. Le Berre, *J. Mater. Res.* **2013**, *28*, 2147 – 2153.
[30] M. Nyman, T. M. Alam, S. K. McIntyre, G. C. Bleier, D. Ingersoll, *Chem. Mater.* **2010**, *22*, 5401 – 5410.
[31] L. Truong, V. Thangadurai, *Chem. Mater.* **2011**, *23*, 3970 – 3977.
[32] G. Larraz, A. Orera, M. L. Sanjuan, *J. Mater. Chem. A* **2013**, *1*, 11419 – 11428.
[33] L. Truong, J. Colter, V. Thangadurai, *Solid State Ionics* **2013**, *247 – 248*, 1 – 7.
[34] F. Gam, C. Galven, A. Bulou, F. Le Berre, M.-P. Crosnier-Lopez, *Inorg. Chem.* **2014**, *53*, 931 – 934.
[35] L. Truong, V. Thangadurai, *Inorg. Chem.* **2012**, *51*, 1222 – 1224.
[36] F. Wang, J. Graetz, M. S. Moreno, C. Ma, L. Wu, V. Volkov, Y. Zhu, *ACS Nano* **2011**, *5*, 1190 – 1197.
[37] D. Rettenwander, C. A. Geiger, G. Amthauer, *Inorg. Chem.* **2013**, *52*, 8005 – 8009.
[38] S. J. Pennycook, *Annu. Rev. Mater. Sci.* **1992**, *22*, 171 – 195.
[39] J. Wolfenstine, J. Sakamoto, J. L. Allen, *J. Mater. Sci.* **2012**, *47*, 4428 – 4431.

